IEEE Access
Multidisciplinary | Rapid Review | Open Access Journal

Received May 3, 2019, accepted May 18, 2019, date of publication May 22, 2019, date of current version June 5, 2019.

Digital Object Identifier 10.1109/ACCESS.2019.2918291

Waveguide Energy-Selection-Filter Switch Array

ZHAOFENG WU, MINGTUAN LIN, JIBIN LIU, AND JIHONG ZHANG, (Student Member, IEEE)
College of Electronic Science and Technology, National University of Defence Technology, Changsha 410072, China
Corresponding author: Jibin Liu (liujibin@nudt.edu.cn)

ABSTRACT This paper presents a waveguide energy-selection-filter switch (ESFS) array for high-power microwave protection, which has a nonlinear transmission response depending on the power intensity of the incident wave. A prototype of nine unit-cells loaded with pin diodes is designed and measured. First, the relationship between the unit-cell dimension and frequency response is analyzed by the full-wave simulation, and an equivalent circuit is studied with numerical fitting. Then, the non-linear characteristics of the unit-cell for different power levels are observed by using an electric field probe. Subsequently, the array structure is designed with equivalent circuits made to evaluate the performance and the coupling effects between the array elements. At the same time, the influence of the number of elements on the transmission coefficient is discussed. Finally, the nonlinear and adaptive transmission characteristics of the ESFS array are demonstrated by the waveguide measurements, which show an isolation improvement of 19.5 dB for high-power microwave protection compared to a single ESFS unit. In addition, the protecting band is wider than that of a single unit.

INDEX TERMS Adaptive protection, energy-selection-filter, high power microwave, pin diode loaded, waveguide.

I. INTRODUCTION

High power microwave (HPM) and electromagnetic pulse (EMP) equipments could generate high energetic pulses with a burst of electromagnetic radiation [1], which may couple to electronic and electrical systems and cause sensitive receiver sensors and other electronic instruments [2]. The main ways of electromagnetic energy coupling with equipment are ''front door'', such as antennas and sensors [3], and ''back door'', like cables and crevices [4]. In order to protect sensitive and vulnerable devices from HPM damage, it is necessary to strengthen and protect both the front and back doors of the equipment. For the threat of back door, increasing isolation of the coupling path is the most effective method, including shielding, lapping, filtering, grounding, absorbing and so on [5]. However, the above methods cannot be used to prevent HPM at front door, of which the main function is to convert and transmit signals through radio waves.

At present, most front door protection is concentrated at the circuit level. Out-of-band HPM and EMP energy can be attenuated by band-pass filters [6], [7], while the protection of sensitive components against in-band high power threats is usually dependent on power limiters [8]–[10]. In order to expand the methods of protecting against the risk of strong electromagnetic pulse, researchers have also studied the protection technology in terms of space field [11], [12], which is different from the circuit.

In recent years, metasurfaces and metamaterials used in HPM and EMP protection also draw increasing attentions. For example frequency selective surface (FSS), a single or multilayer structure consisting of period resonance units, is able to transmit in-band EM incidence while reflect out-band wave, function as a filter [13]–[15]. Adjustable FSSs have been designed by loading varactor or switch diodes with DC bias on traditional FSS [16]–[18], of which the frequency band and transmission coefficient can be changed by adjusting DC bias. And yet without self-adaptive dependent on energy, FSS has no energy-selective properties and cannot protect against high power electromagnetic pulse (EMP) in the pass-band. Then, Yang Cheng et al. first reported the energy selective surface (ESS), like a limiter, with pin-diode for EMP protection, which only sensitive to the power density or field intensity of incident wave [12], [19], [20]. Subsequently, a spatial power limiter using a nonlinear FSS was researched combining the frequency selection characteristics of FSS and the energy selection characteristics of ESS [21], [22]. However, as planar structures, aforementioned structures should be implemented at the front end

The associate editor coordinating the review of this manuscript and approving it for publication was Feng Lin.

of antenna to defend HPM and HPEM threats, just like a radome, which takes a lot of space and will inevitably affect the radiation of antenna [23].

In comparison with circuit level and space field protection, waveguide protection device is another effective method to avoid HPM attack. Waveguide is a kind of transmission line with large power capacity and small loss, which is often used as a bridge between horn antenna of radar and system. Researchers have designed a series of waveguide protection component, including waveguide diode limiter [24], ferrite limiter [25], plasma waveguide limiter [26] and so on. A waveguide passive power limiter with H-shaped resonant aperture was proposed in [27], which combined structure of a BPF and a limiter. However, aforementioned component needs to be fixed in the waveguide and cannot be replaced, limiting its application. Recently, we had reported a narrow-band waveguide energy-selective filter with only one unit and one diode, is pluggable and can provide more design freedom [28]. Subsequently, we studied the energy selective surface of multi-element based on the high impedance surface in waveguide, which adaptively adjusts the impedance of waveguide wall according to different power to protect HPM from attack [23]. However, its protective capability is insufficient and isolation is only 13 dB at high power.

Based on our previous the work, we proposed an Energy-Selection-Filter Switch array (ESFS) for HPM protection with higher isolation and wider protecting band, which is self-adaptive depending on the magnitude of incident wave energy. Compared with other traditional waveguide limiters and filters, the proposed ESFS does not need to change the structure of the original waveguide, that is to say, it is pluggable and replaceable. The isolation effect under high power signal is better than that of [23] and the frequency bandwidth wider than that of [28].

II. CELL STRUCTURE AND WORKING MECHANISM

A. STRUCTURE OF CELL

The unit cell proposed is illustrated in Fig.1, which consists of three parts, the intermediate circuit (sub #2), and the top (sub #1) and bottom (sub #3) metal patches. They are all made by printed circuit boards (PCB), and the copper is

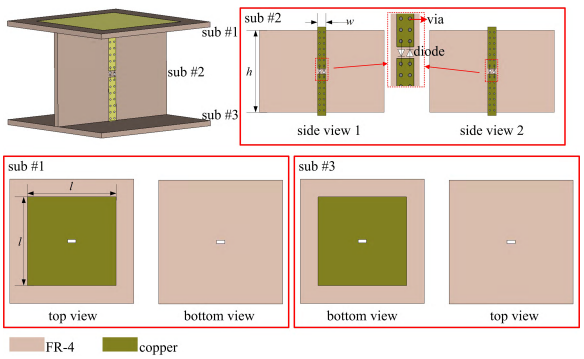

FIGURE 1. Geometry of the unit cell in proposed ESFS.

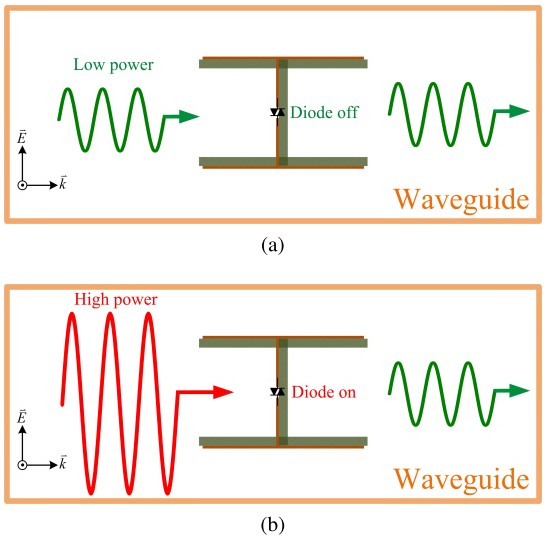

FIGURE 2. Schematic model of the proposed ESFS at the condition of (a) low power and (b) high power.

printed respectively on the FR-4 substrate with permittivity of 4.5 and thickness of 0.8 mm. The top and bottom patches are exactly the same in length and width ($l \times l$). Besides, these two thin metallic patches are separated by air and connected by another PCB with a metal line (the length and width are h, w respectively). The diode is loaded in the middle gap. The structure of sub #2 is different from that of [23]. The middle metal wires of sub #2 are on both sides of PCB, and are effectively connected through vias in the middle, which helps to connect multiple diodes to provide greater power capacity and smaller on-resistance. And pin diodes are loaded as external lumped elements to perform the nonlinear properties on different conditions. In order to make the middle circuit short-circuited effectively in both positive and negative half-cycles of high power signals, four diodes were loaded at the both sides of the metal line gap of sub #2.

B. WORKING MECHANISM OF THE PROPOSED ESFS

The mechanism of this energy-dependent filter is mainly based on the capacitor and inductance (LC) resonant filter in waveguide. Fig.2 depicts the schematic of proposed ESFS. The structure is composed of two sub-wavelength metallic patches and a metallic wire, which are connected by pin diodes to achieve nonlinear performance. In waveguide, the two patches form capacitances with the top and bottom metal walls of the waveguide, respectively. Meanwhile, the metallic wire is equivalent to an inductance connecting two capacitors in series. When TE10 mode electromagnetic wave is input, strong electric field is excited between patch and waveguide wall, while strong magnetic field is excited around metal wire. The intensity of electric field and magnetic field stimulated by different incident power is different, that is, the voltage levels loaded on both ends of the diodes are different. Thus, the proposed ESFS perform different transmission characteristics.

If the voltage induced by incident wave is not high enough to turn on the pin diode, the resistance for ideal pin diodes in off-state is infinite. The equivalent circuit is open and only two patches are placed parallel in the middle of the waveguide without being connected, which cannot form a complete resonant circuit. Thus, the proposed ESFS does not have the ability of frequency selection and signals of all frequency (permissible transmission frequency of waveguide) can be transmitted with lower loss. This insertion loss is mainly caused by leakage current in diode and dielectric loss of PCB. In order to reduce the loss, high isolation diode and low loss substrate are prerequisite.

On contrast, high power electromagnetic waves can excite enough voltage to turn on the diode. The on-resistance of ideal diode is zero in the positive biasing status (on-state), which connects the two patches and the wire. Equivalent capacitors of two patches and inductor of the wire are connected in series and then they are paralleled on the transmission line. Therefore, it can resonate at the set frequency and reflect the energy, thus protecting the back-end circuit or equipment. At this time, the isolation effect of the ESFS depends on the on-resistance of the diode. That is to say, it is expected that the diode could always be in the on-state and exhibit low resistance. To ensure the stable on-state and low forward resistance of diodes, two pin diodes should be placed reversely.

C. EQUIVALENT CIRCUIT STUDY OF CELL

As analyzed above, ESFS exhibits full-pass and low insertion loss characteristics under small signal conditions, the mechanism of which is simple. However, it is needed to be analyzed band-stop characteristics and equivalent circuit models when high power signal is inputted.

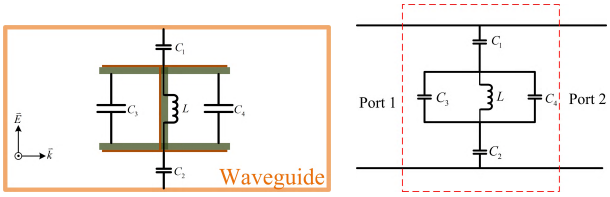

FIGURE 3. Equivalent Circuit of unit-cell in waveguide under high power condition.

As shown in Fig.3, when voltage excited by the high power signal is enough to turn on the diodes, the whole unit structure is equivalent to the series resonant circuit of capacitors and inductors. In general, capacitance mainly stores electric field energy, while inductance mainly stores magnetic field energy. Fig.4 (a) and (b) show the simulation results of electric field density and magnetic field density, respectively. Obviously, the magnetic field energy between the two patches is concentrated, while the electric field energy is very strong not only between patches, but also between the patch and the waveguide wall. Thus, the top metal and the upper wall of the waveguide are equivalent to a parallel plate capacitor C_1, and

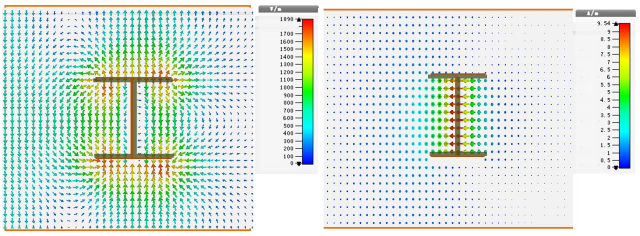

FIGURE 4. (a) Electric field and (b) magnetic field distribution.

the bottom is equivalent to a capacitor C_2 similarly. Meanwhile, two coupling capacitances between the two metallic patches are C_3 and C_4. According to the law of parallel plate capacitors, the value of capacitance depends on the size and distance of parallel plate electrodes. The metallic wire inserted in the middle is equivalent to inductor L, which is connected by diodes. Finally, C_1, C_2, C_3, C_4 and L form a series resonant circuit. The resistance of the ideal diode is zero as discussed above when diode is turned on. In order to study the pass-band characteristics of the structure simply, it can be considered that the metal wire in the middle is a perfect connection between the top and bottom metal patches. Therefore, when the high power signal is input, the diode is turned on and the whole structure in the waveguide is equivalent to the resonant circuit as shown in Fig.3. Then the impedance Z_s of the proposed ESFS is given by

$$\begin{aligned} Z_s &= \frac{1}{j\omega C_1} + \frac{1}{j\omega C_2} + \left(\frac{1}{j\omega C_1} \| \frac{1}{j\omega C_2} \| j\omega L\right) \\ &= \frac{1 - (C_3 + C_4 + \frac{C_1 C_2}{C_1 + C_2})\omega^2 L}{j\omega \frac{C_1 C_2}{C_1 + C_2} - j\omega^3 L \frac{C_1 C_2}{C_1 + C_2}(C_3 + C_4)} \end{aligned} \tag{1}$$

where $C = C_3 + C_4 + \frac{C_1 C_2}{C_1 + C_2}$, refers to the combining effect of C_1, C_2, C_3 and C_4. Thus, the input impedance becomes zero at the resonant frequency ω_0, which is

$$\omega_0 = \frac{1}{\sqrt{LC}} \tag{2}$$

The capacitance C is determined by the area ($S = l \times l$) and the distance h between the patches and waveguide wall. Besides, the inductance L is related to the width w and length h of the metal line on the sub #2. Therefore, by adjusting these parameters, the equivalent inductance and capacitance can be adjusted to change the resonant frequency.

Firstly, the initial structure parameters of the cell are determined. The length l of the metal patch on sub#1 and sub#3 is 16 mm. The distance between sub#1 and sub#3 is 15 mm, which is the same as the height h of sub#2. And the width w of metal line on sub#2 is 2 mm. Then the cell is placed in the middle of a waveguide and the perimeter of the waveguide is referred to the standard waveguide WR430, which has a width of 109.22 mm and a height of 54.61 mm, and a bandwidth from 1.72 GHz to 2.61 GHz. The full wave simulation is carried out by software of Computer Simulation Technology

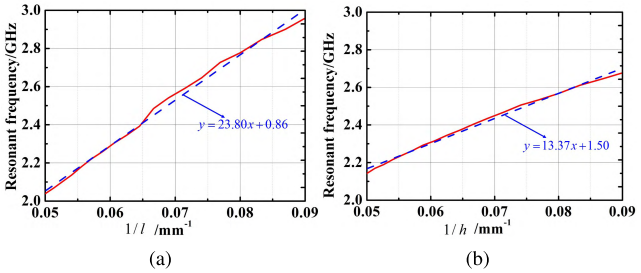

FIGURE 5. The linear relationship between resonance frequency and (a) $1/l$, (b) $1/h$.

(CST), and the walls of waveguide are set as PEC. By changing the length l and distance h (both from 10 mm to 20 mm with a step 0.5 mm) respectively, the variation of resonant frequency can be obtained with CST as shown in Fig.5. Subsequently, the first-order function curves obtained by numerical fitting of the simulation results are also shown in the figure, which is in good agreement with the simulation results. The resonant frequency is proportional to $1/l$, that is to say, inversely proportional to patch size l. That is because the capacitance C_1 and C_2 increase with the patch size. Similarly, the resonant frequency also decreases with the increase of patch distance h. The equivalent circuit value of the single cell has been discussed in our early report [28], which will be used to analyze equivalent circuit with multi-unit structure in this article.

D. NONLINEAR CHARACTERISTICS OF LOADED DIODES

In the preceding section, the band-stop characteristics of the proposed ESFS are analyzed, which is assumed that the ideal diode is turned on. However, the switching state of the diode is determined by the input power and ESFS structure. In this section, the voltage at both ends of the diode and the time-domain response of the structure at different input power levers are studied.

In this design, a silicon PIN diode of BAP-51-02 from NXP Corporation is selected, which has low parasitical-capacitances, short switching time and small on-resistance. The diodes 51-02 have an approximate capacitance of 0.15 pF at off-state, while it is equivalent to a series of resistor 0.7 Ω and inductor 0.77 nH at on-state. In the simulation, lumped element capacitors or inductors and resistors are used to replace the on- and off-state of the diodes, respectively.

To observe the input and output waveforms of continues wave in time domain, simulations with low power and high power are carried out. The normalized voltage of input and output wave are recorded at the same time and shown in Fig.6. As shown in Fig.6 (a), when the input power level is relatively low, magnitude of input and output wave are almost the same, which means that waves propagate through the waveguide with very low insertion loss. While on the condition of high power input, there is an obvious difference between the magnitude of input and output signal as shown

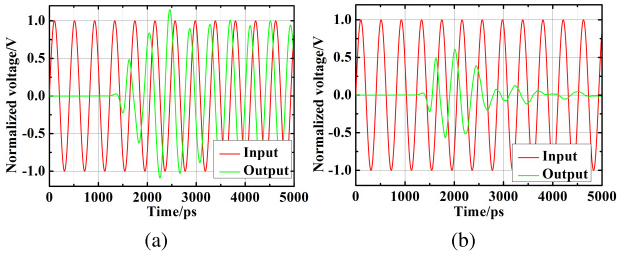

FIGURE 6. Input and output normalized voltage with diodes (a) off and (b) on.

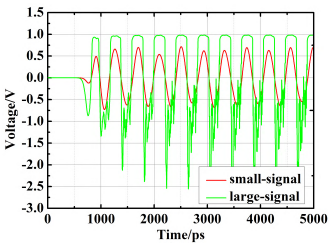

FIGURE 7. Voltage at both ends of the diode in the case of large signal and small signal.

in Fig.6 (b). Such results have proved the HPM prohibition ability of proposed ESFS.

Subsequently, the probe was used to detect the voltage changes at both ends of the diode at different input power as shown in Fig.7. When the small signal is input, the wave at both ends of the diode behaves as a complete sinusoidal wave. This proves that the small signal cannot turn on the diodes, and thus cannot form a complete resonant circuit. So small signals can pass through with low loss. However, it is obvious that the waveforms at both ends of the diode are distorted when the large signal inputs. According to the manual of the diode 51-02, its forward voltage is 0.95 V, thus the positive half-cycle voltage is limited to less than 1 V, which is consistent with the simulation.

III. STUDY AND DESIGN OF ESFS ARRAY

As analyzed in the previous section, one unit cell can only form one zero point, which is just like a narrow-band filter. After loading the non-linear elements (diodes), it can only protect against the high power energy of the narrow-band. However, high power microwave signals are usually broadband, so the design of broad-band band-stop filters is necessary. Multiple resonant points or wide bandwidth can be obtained by connecting multiple units of different sizes in series or parallel. That is to say, different sizes of structures can form multiple zero points of interest, so broadband filters can be designed to prevent high power energy. The schematic diagram of multi-unit series connection in waveguide is shown in Fig.8. In this paper, the perimeter of the waveguide is referred to the standard waveguide WR430, which has a width of $a = 109.22$ mm, a height of $b = 54.61$ mm, and a bandwidth from 1.72GHz to 2.61GHz.

For multi-cell structure, there will be a coupling capacitance between two patches between adjacent cells. When the

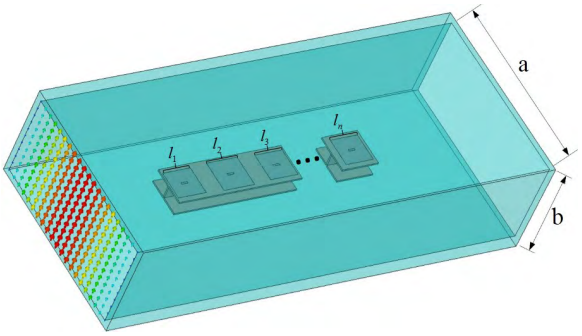

FIGURE 8. Diagram of multi-unit cascade connection in waveguide.

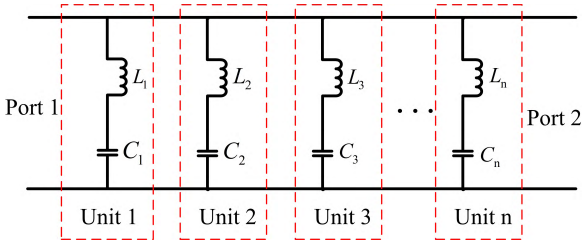

FIGURE 9. Equivalent Circuit without interstage coupling.

period of structure is larger than one wavelength of waveguide, that is, the distance d between adjacent cells is larger than the wavelength λ_g, and the coupling capacitance is small enough to be neglected. While the distance d between adjacent cells is small, the influence of coupling must be considered.

A. WEAK COUPLING BETWEEN ADJACENT ELEMENTS

When the adjacent units are far away, the adjoining element patches are weakly coupled. At this time, the design only needs to consider the resonance characteristics of each cell separately and multiple resonant zero points can be freely combined to form a wide-band or multi-band filter. After simplifying the circuit in Fig.3, the equivalent circuits of n cell arrays can be obtained by series connection as shown in Fig.9, which does not consider the coupling between stages because the element is far away. The equivalent capacitance and inductance of each unit can be obtained by the study of a single unit-cell in the preceding section.

In order to design an ESFS with dual stop-bands, two units with different sizes are placed in the waveguide for simulation. One cell size are $l_1 = 22$ mm, $h_1 = 8$ mm, and the other cell dimension are $l_2 = 20$ mm, $h_2 = 0.8$ mm. Their resonant frequencies are 2.13 GHz and 2.45 GHz respectively when they exist alone in the waveguide. And $C_1 = 2.5$ pF and $L_1 = 2$ nH are the equivalent capacitance and inductance of unit 1, while the two parts of unit 2 are $C_2 = 2.1$ pF and $L_2 = 2$ nH, respectively. Full-wave simulation and circuit simulation are carried out through Computer Simulation Technology (CST) and Advanced Design System (ADS), respectively. The result of three-dimensional full-wave simulation shows that two stop-bands can be obtained by cascading two different size units in the case of weak coupling as shown in Fig.10 (a).

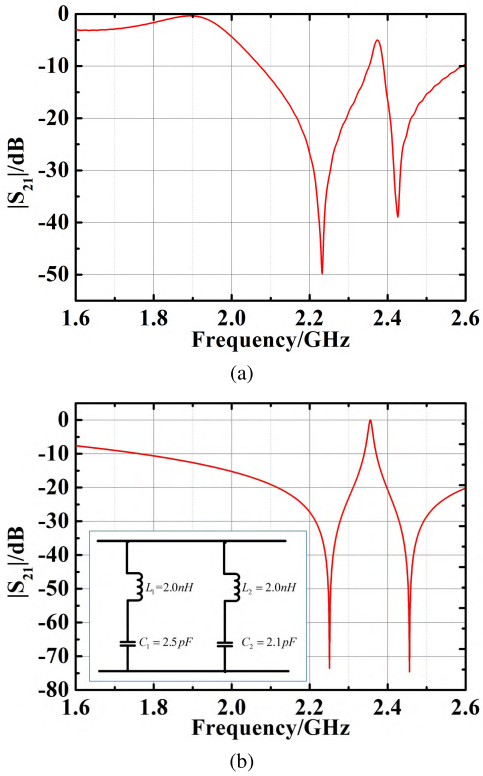

FIGURE 10. Dual units with near bandstop simulation by (a) CST and (b) ADS.

At the same time, the zero points of equivalent circuit simulation shown in Fig.10 (b) is consistent with that of full-wave simulation. However, the passband between the two zero points of the circuit simulation curve is different from that of the three-dimensional simulation, especially at 2.35 GHz. That is because the effect of waveguide between two units is not considered in the equivalent circuit. In addition, the ideal lumped elements used in equivalent circuits have high quality factor. This simple equivalent circuit is sufficient to analyze the stop-band characteristics of two zero points. Subsequently, on the basis of the above structure, the size of the first unit patch is changed to $l_1 = 30$ with other dimensions remaining unchanged. According to the analysis of the relationship between cell structure and frequency response in the previous section, the change of patch size mainly affects the equivalent capacitance, so only the capacitance of the first stage is changed in the equivalent circuit as shown inside of Fig. 11. At this time, the resonant zero point of the first stage is 1.73 GHz. Through full-wave simulation and equivalent circuit simulation, the transmission coefficients are obtained as shown in Fig.11. Compared with the previous simulation results, it is obvious that the passband between two zero points in circuit simulation has a pole at 2.1 GHz, which once again explains that the lumped element in circuit simulation has a higher quality factor. It is the reason why the equivalent circuit simulation and full-wave simulation are different in passband.

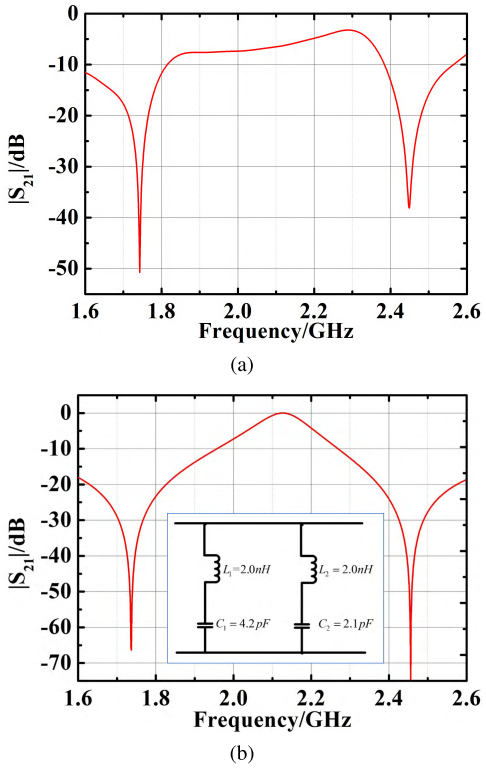

FIGURE 11. Dual units with two stop-band simulation by (a) CST and (b) ADS.

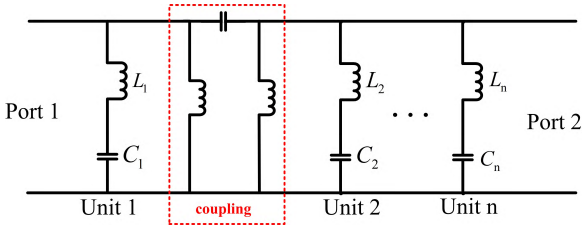

FIGURE 12. Equivalent Circuit with interstage coupling.

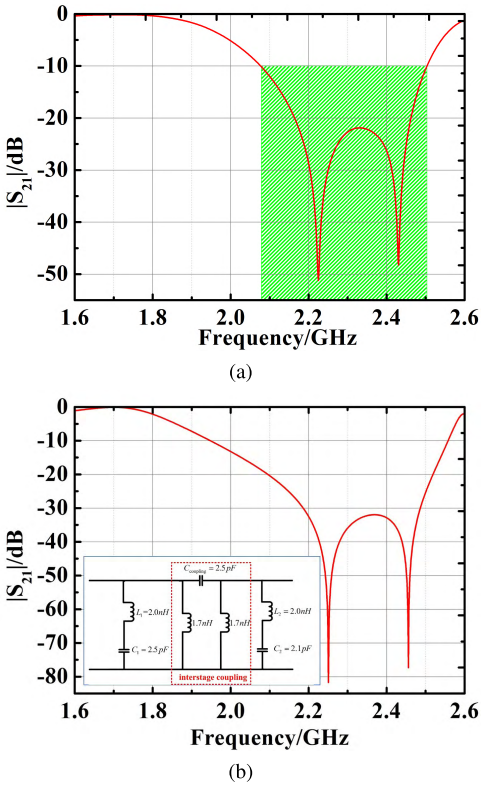

FIGURE 13. Dual units with wideband bandstop simulation by (a) CST and (b) ADS.

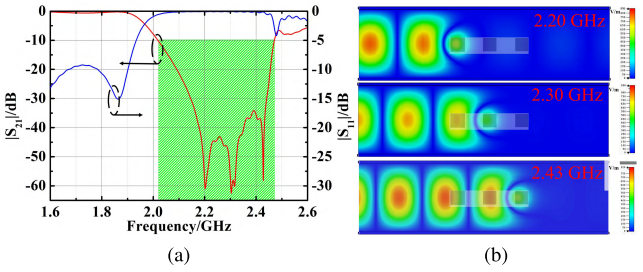

FIGURE 14. (a) Transmission coefficient and reflection coefficient of three-element full-wave simulation. (b) Electric field distribution of three-unit structure.

B. STRONG COUPLING OF ADJACENT ELEMENTS

According to the previous simulation results, weakly coupled elements can form a multi-band stopband filter, but cannot against broadband high power signals. When the two elements are close to each other, there will be a coupling capacitance between the patches of the two adjacent elements and two coupling inductance [23] as shown in Fig.12. The distance between the two units is reduced to one-tenth of the waveguide wavelength and a bandstop filter with a bandwidth of 0.5 GHz is obtained, the results of which show that the frequency band between two zero points becomes stopband by simulation with CST and ADS as shown in Fig.13.

In order to make the in-band attenuation larger, a zero point can be added to the in-band, that is, a unit can be added on the basis of strong coupling. Result of transmission and reflection coefficients by full-wave simulation with patch dimension of $l_1 = 21$ mm, $l_2 = 22$ mm and $l_3 = 20$ mm is shown in Fig.14 (a). Compared with Fig.13, the attenuation in the stopband of three elements is greater, which can provide better protection effect. Besides, reflection coefficient is close to 0 dB in stopband, which shows that the high power signal is almost totally reflected. Subsequently, the electric field distribution in waveguide at different frequencies are simulated, which further illustrates that the electromagnetic waves of different frequencies only resonate and reflect at the corresponding size units in Fig.14 (b). What's more, the electric field distribution indicates that standing waves are formed on the incident side of the waveguide, so the energy is reflected and cannot through the proposed ESFS, thus providing electromagnetic protection for the following devices.

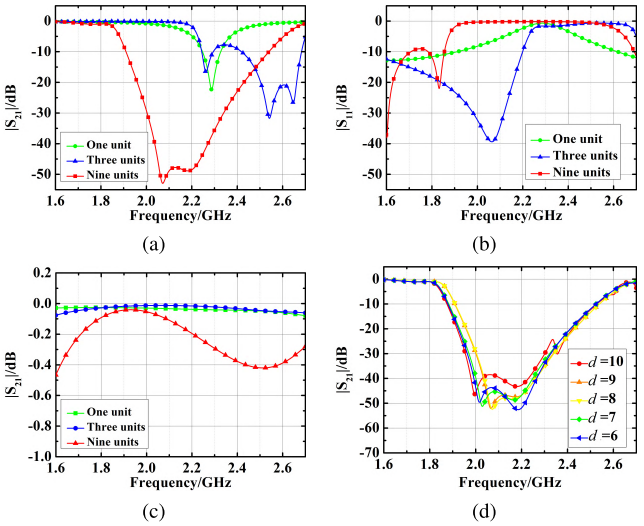

FIGURE 15. (a) Transmission and (b) reflection coefficient with diodes on and (c) insertion loss with diodes off. (d) Transmission coefficient with difference distance between every two layers when diodes on.

C. COMPARISON WITH SINGLE UNIT

The isolation and insertion losses can be obtained by simulation with the equivalent lumped parameters of large and small signals of 51-02 diode, respectively. Fig.15 (a) and (b) show the transmission curves and reflection coefficient of one unit and multiple units when the diode is on. Obviously, the stopband bandwidth of three cells is wider than that of one cell, while the insertion loss is the same when the diode is off as shown in Fig. 15 (d). However, the maximum isolation of stop band is only 30 dB. In order to further increase the isolation on high power condition and the withstand power of the component, three identical structures are placed in parallel horizontally to form a 3*3 units array. The simulation results show that nine units array has higher isolation and wider bandwidth than three units array under high-power signals as shown in Fig.15 (a) and the signal in stopband is reflected as shown in Fig.15 (b), of course, the loss will increase inevitably as shown in Fig.15 (c).

When the structure of three layers is placed in parallel, coupling effect comes into being between adjacent layers. Thus, transmission coefficient and frequency response may be influenced by changing the distance d of every two layers, which affects the coupling effect. Due to the limit of the waveguide size in this frequency band, d could not be adjusted with no limit. Based on this, transmission coefficients are simulated by CST with d from 6 mm to 10 mm as shown in Fig.15 (d). As the distance between layers increasing, there is no significant change in transmission characteristics. Although the coupling capacitance between layers increases when the three layers are close to each other, the other capacitive coupling between patch and waveguide wall in the top and lower layers is reduced. As a result, the frequency response does not change significantly.

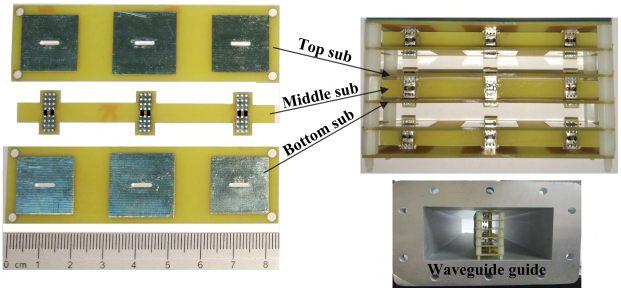

FIGURE 16. Prototype fabricated by printed circuit board technology.

IV. EXPERIMENT AND RESULTS

In order to verify the feasibility, a prototype is fabricated by printed circuit board technology as shown in Fig.16. The prototype consists of three layers connected by nylon spacer, each of which has the same structure with $l_1 = 18$ mm, $l_2 = 20$ mm, $l_3 = 18$ mm and $h = 8$ mm. For convenience, the same height of nylon spacer is used to connect each cell and each layer, which is 8 mm. Meanwhile, the position of the ESFS in the waveguide is also shown in the Fig.16. Subsequently, a test experiment was carried out and the experimental setting for testing the prototype in the waveguide with different power is shown in Fig.17. The signal of the Vector Network Analyzer (VNA) is amplified by the Power Amplifier (PA) and then enters the waveguide through the Isolator to prevent the reflection energy of the ESFS from damaging the PA. At the output port of the waveguide, the signal enters the VNA through the attenuator. Therefore, this experiment can only obtain the transmission coefficient, but not the reflection coefficient. Transmission coefficients at different input power levels are measured and shown in Fig.18. When the power into the waveguide is below 35 dBm, voltages induced are

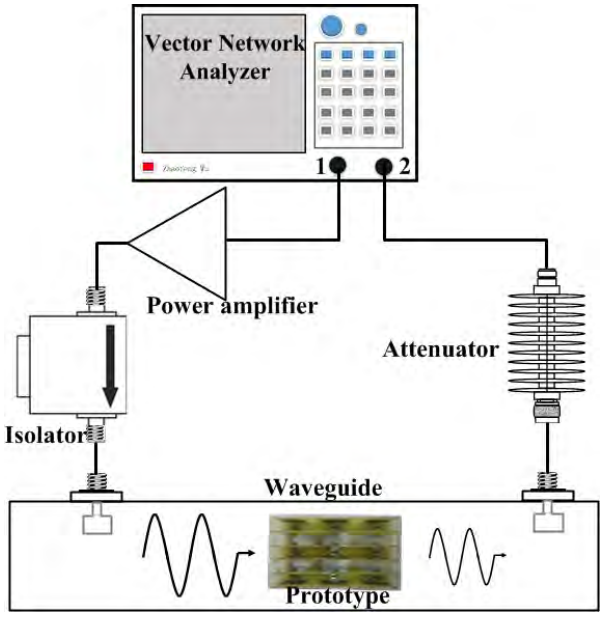

FIGURE 17. Experimental setup of waveguide measurement.

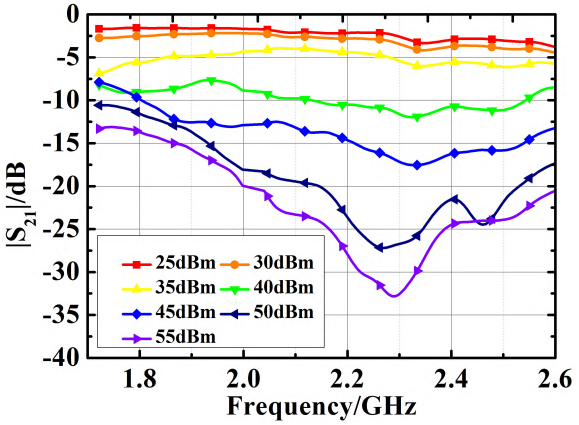

FIGURE 18. Measurement of transmission coefficient with signals at different input power.

not enough to turn on pin diodes and circuit can't resonate. On this condition, the signal can pass with low loss at the interest frequency and the curves of transmission coefficient are similar.

With the increase of the power outputting from Power Amplifier, the electric field density in waveguide and the voltage at both ends of the diode gradually increase. Until the input power is 55 dBm, the diodes are fully turned on and the component exhibits broadband band-stop characteristics. Within the whole waveguide frequency range (1.72-2.61 GHz), the isolation is greater than 12.5 dB, especially at 2.3 GHz, the isolation reaches 32.5 dB. There are a little difference between measurement and simulation in Fig. 15 at the three resonant points because the static equivalent parameters of the diode are used in the simulation, while diode values of equivalent lumped elements will fluctuate with the variation of applied voltages and frequency. Besides, it is manually welded and assembled, the actual size of the prototype cannot be strictly consistent with that of simulation, which affects the distribution capacitance and inductance parameters of the structure. The small change of capacitance could change the resonant frequency of a single unit [28], and then affect the frequency response of the whole structure. The results have verified the nonlinear characteristics of proposed ESFS that the transmission coefficient is dependent on the power intensity of incident wave.

V. CONCLUSION

A waveguide ESFS was designed in this paper for HPM protection by reflecting the over-threshold high-power incident wave. The working mechanism of ESFS unit is analyzed, and the relationship between structure size and frequency characteristics is studied by numerical method. At the same time, the equivalent circuit of ESFS is studied, which is helpful for structure design. Subsequently, the non-linearity of the cell structure is simulated and the time-domain waveforms of the diode and waveguide ports under different power conditions are observed by using the probe. In order to expand the bandwidth, a cascaded multi-cell array is proposed and simulated. Finally, the prototype of array structure is made and measured. The measurement results show that the proposed ESFS has better protection ability in the waveguide operating frequency range, and the isolation reaches 32.5 dB at 2.3 GHz. Compared with other traditional waveguide limiters and filters, the proposed ESFS does not need to change the structure of the original waveguide, that is to say, it is pluggable and replaceable. The isolation effect under high power signal is better than [23] and the frequency bandwidth wider than [28]. Therefore, the ESFS proposed in this paper can provide a different way to protect HPM.

REFERENCES

[1] D. V. Giri and F. M. Tesche, "Classification of intentional electromagnetic environments (IEME)," *IEEE Trans. Electromagn. Compat.*, vol. 46, no. 3, pp. 322–328, Aug. 2004.
[2] G. Ni, B. Gao, and J. Lu, "Research on high power microwave weapons," in *Proc. Asia–Pacific Microw. Conf. (APMC)*, vol. 2, Jan. 2006, p. 4. doi: 10.1109/APMC.2005.1606492.
[3] Y. Liu, C. Chai, Q. Fan, C. Shi, X. Xi, X. Yu, and Y. Yang, "Ku band damage characteristics of GaAs pHEMT induced by a front-door coupling microwave pulse," *Microelectron. Rel.*, vol. 66, pp. 32–37, Nov. 2016.
[4] S.-T. Song, H. Jiang, and Y.-L. Huang, "Simulation and analysis of HEMP coupling effect on a wire inside an apertured cylindrical shielding cavity," *Appl. Comput. Electromagn. Soc. J.*, vol. 27, no. 6, pp. 505–515, Jun. 2012.
[5] J. Gao, J. Luo, L. Wang, X. Huang, H. Wang, X. Song, M. Hu, L.-C. Tang, and H. Xue, "Flexible, superhydrophobic and highly conductive composite based on non-woven polypropylene fabric for electromagnetic interference shielding," *Chem. Eng. J.*, vol. 364, pp. 493–502, May 2019.
[6] K. Bi, X. Wang, Y. Hao, M. Lei, G. Dong, and J. Zhou, "Wideband slot-coupled dielectric resonator-based filter," *J. Alloys Compound*, vol. 785, pp. 1264–1269, May 2019.
[7] J. Jing, X. Wang, L. Lu, L. Zhou, H. Shu, X. Wang, and J. Chen, "Reconfigurable RF notch filter based on an integrated silicon optical true time delay line," *J. Phys. D, Appl. Phys.*, vol. 52, no. 19, May 2019, Art. no. 194001.
[8] H. Patel, K. Kellogg, H. Morales, L. Dunleavy, R. Jones, and P. Head, "Nonlinear modeling of a high peak power PIN limiter," *Microw. J.*, vol. 62, no. 1, p. 60, Jan. 2019.
[9] R. Pascaud, F. Pizarro, T. Callegari, L. Liard, O. Pigaglio, and O. Pascal, "Low insertion loss microplasma-based limiter integrated into a microstrip bandpass filter," *Electron. Lett.*, vol. 51, no. 14, pp. 1090–1092, Jul. 2015.
[10] A. Semnani, S. O. Macheret, and D. Peroulis, "A high-power widely tunable limiter utilizing an evanescent-mode cavity resonator loaded with a gas discharge tube," *IEEE Trans. Plasma Sci.*, vol. 44, no. 12, pp. 3271–3280, Dec. 2016.
[11] A. A. Omar and Z. Shen, "Thin 3-D bandpass frequency-selective structure based on folded substrate for conformal radome applications," *IEEE Trans. Antennas Propag.*, vol. 67, no. 1, pp. 282–290, Jan. 2019.
[12] C. Yang, P. G. Liu, and X. J. Huang, "A novel method of energy selective surface for adaptive HPM/EMP protection," *IEEE Antennas Wireless Propag. Lett.*, vol. 12, pp. 112–115, 2013.
[13] L. Ge-Wu, J. Zhang, J.-Y. Yang, T.-X. Zhang, and Y. Kou, "Status and development of frequency selective surface radome," *Acta Phys. Sinica*, vol. 62, no. 19, p. 198401, Oct. 2013.
[14] B. Munk, "Frequency selective surfaces: Theory and design [book review]," *IEEE Signal Process. Mag.*, vol. 18, no. 1, p. 94, Jan. 2001.
[15] H. Zhang, C. Hu, J. Yang, L. Tang, D. Huang, L. Shao, M. Piao, C. Li, and H. Shi, "Graphene-based active frequency selective surface in microwave frequency," *J. Appl. Phys.*, vol. 125, no. 9, Mar. 2019, Art. no. 094501.
[16] Y. N. Kazantsev, G. A. Kraftmakher, and V. P. Mal'tsev, and I. P. Nikitin, "Elements of frequency-selective surfaces with a wide tuning range of the resonance frequency," *J. Commun. Technol. Electron.*, vol. 62, no. 12, pp. 1343–1348, Dec. 2017.
[17] Y. Rahmani-Shams, S. Mohammd-Ali-Nezhad, A. N. Yeganeh, and S. H. Sedighy, "Dual band, low profile and compact tunable frequency selective surface with wide tuning range," *J. Appl. Phys.*, vol. 123, no. 23, Jun. 2018, Art. no. 235301.
[18] B. Yi, P. Liu, Q. Zhou, and T. Fan, "A miniaturized absorptive/transmissive radome with switchable passband and wide absorbing band," *IEICE Trans. Commun.*, vol. 100, no. 5, pp. 788–792, May 2017.

[19] K. Wang, P. Liu, Y. Qin, J. Huang, and B. Yi, "A miniaturized self-actuated bandpass protection structure based on energy low-pass mechanism," in *Proc. Int. Symp. Electromagn. Compat.-EMC EUROPE*, Angers, France, Sep. 2017, pp. 1–4.
[20] S. Monni, D. J. Bekers, M. van Wanum, R. van Dijk, A. Neto, G. Gerini, and F. E. van Vliet, "Limiting frequency selective surfaces," in *Proc. Eur. Microw. Conf.*, Sep./Oct. 2009, pp. 606–609.
[21] Z. Chen, X. Chen, and G. Xu, "A spatial power limiter using a nonlinear frequency selective surface," *Int. J. RF Microw. Comput.-Aided Eng.*, vol. 28, no. 4, May 2018, Art. no. e21205.
[22] F. Deng, X. Xi, J. Li, and F. Ding, "A method of designing a field-controlled active frequency selective surface," *IEEE Antennas Wireless Propag. Lett.*, vol. 14, pp. 630–633, 2015.
[23] J. Zhang, M. Lin, Z. Wu, L. Ding, L. Bian, and P. Liu, "Energy selective surface with power-dependent transmission coefficient for high-power microwave protection in waveguide," *IEEE Trans. Antennas Propag.*, vol. 67, no. 4, pp. 2494–2502, Apr. 2019.
[24] N. B. Gudkova and A. S. Shnitnikov, "Millimeter-wave waveguide dioide limiter," in *Proc. 16th Int. Crimean Microw. Telecommun. Technol.*, vol. 1, Sep. 2006, pp. 123–124.
[25] J. Helszajn, R. W. Murray, E. G. S. Davidson, and R. A. Suttie, "Waveguide subsidiary resonance ferrite limiters," *IEEE Trans. Microw. Theory Techn.*, vol. 25, no. 3, pp. 190–196, Mar. 1977.
[26] G. Yang, J. C. Tan, D. Y. Sheng, and Y. C. Yang, "Gas selection and calculation of its breakdown field for plasma waveguide limiter," *High Power Laser Part. Beams*, vol. 20, no. 3, 2008.
[27] Y.-K. Cho, J. S. Park, J. Yeo, J.-I. Lee, and K.-C. Kim, "Compact microwave waveguide limiter," *IEICE Electron. Express*, vol. 13, no. 23, Dec. 2016, Art. no. 20160854.
[28] Z. Wu, M. Lin, J. Zhang, and J. Liu, "Energy selective filter with power-dependent transmission effectiveness in waveguide," *Electronics*, vol. 8, no. 2, p. 236, Feb. 2019.

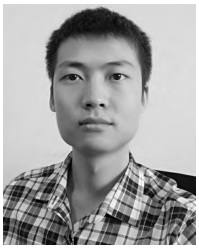

ZHAOFENG WU was born in Baoji, Shaanxi, China, in 1995. He received the B.Eng. degree in electronic engineering from the National University of Defense Technology, Changsha, China, in 2017, where he is currently pursuing the M.E. degree in electronic science and technology under the supervision of Prof. J. B. Liu.

His research interests include millimeter wave antenna, microwave components, and electromagnetic protection.

MINGTUAN LIN received the B.Sc., M.Sc., and Ph.D. degrees in electronic science and engineering from the National University of Defense Technology, Changsha, China, in 2012, 2014, and 2018, respectively, under the supervision of Prof. P. G. Liu.

He has been a Visiting Ph.D. Student with the Queen Mary University of London, London, U.K., since 2015, under the guidance of Dr. Y. Gao. He is currently a Lecturer with the National University of Defense Technology. His current research interests include radio orbital angular momentum, array signal processing, meta-material, and mm-wave antenna design.

JIBIN LIU received the B.Sc. degree in electronics and information system and the M.Sc. and Ph.D. degrees in electromagnetic field and microwave technology from the National University of Defense Technology (NUDT), Changsha, China, in 1995, 1998, and 2007, respectively. He is currently a Professor with NUDT. His current research interests include electromagnetic compatibility and protection, electromagnetic field, and microwave technology.

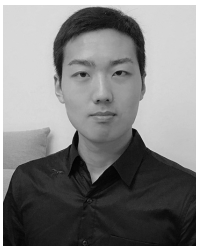

JIHONG ZHANG (S'18) received the B.Eng. degree in electronic engineering and the M.Eng. degree in electronic science and technology from the National University of Defense Technology, Changsha, China, in 2015 and 2017, respectively, where he is currently pursuing the Ph.D. degree in electronic science and technology under the supervision of Prof. P. G. Liu.

His research interests include high-intensity radiation fields metasurface, microwave components, and conformal antenna array.